Optical Properties of Noble Metals. II.*

B. R. COOPER† AND H. EHRENREICH
Division of Engineering and Applied Physics, Harvard University, Cambridge, Massachusetts

AND

H. R. PHILIPP
General Electric Research Laboratory, Schenectady, New York

(Received 25 November 1964)

Earlier work dealing with the optical properties of Cu and Ag is extended along two directions. The optical properties of Au are discussed and interpreted in terms of intra- and interband processes as well as plasma effects as elementary excitations of the system. In addition, the previous tentative interpretation of the low-energy optical structure in terms of interband transitions near L and X in the Brillouin zone is examined carefully by means of absolute calculations of the imaginary part of the frequency-dependent dielectric constant, using as input data the results of band calculations as well as Fermi surface experiments. The agreement of the results for all three noble metals with experiment strongly supports the previous interpretation. It is shown that in metals, sharp optical structure may arise from transitions between relatively flat, filled bands, such as the upper d band, and empty states just above the Fermi surface. This structure complements that arising from transitions at critical points and accounts for the region in the noble metals where direct interband transitions first set in. Finally, the present calculations are used as a basis for comment on recent data of Spicer and Berglund and the relative importance of direct and indirect transitions in photoemission processes.

1. INTRODUCTION

THE optical properties of Cu and Ag extending from the infrared to the far vacuum ultraviolet were discussed and interpreted in a previous paper.[1] The observed structure was attributed to intra- and interband processes, as well as plasma effects. Some prominent pieces of interband structure were tentatively associated with transitions in various regions of the Brillouin zone on the basis of existing band calculations.[2–4]

The present paper extends the previous work in two directions. First, the survey of optical properties of the noble metals is enlarged by a discussion of data for Au along the lines of I. Section 2 is devoted to this topic. Second, the interpretation of the low-energy structure due to interband transitions near L and X in the Brillouin zone made in I is examined carefully by means of absolute calculations of the imaginary part of the frequency-dependent dielectric constant, using as input data the results of band calculations, as well as Fermi surface experiments.[5–8] As discussed in Secs. 3 and 4, the agreement of the results for all three noble metals with experiment is such as to support very strongly the previous interpretation. In this connection, it is shown that in the case of metals, sharp optical structure may arise from transitions between relatively flat, filled bands, such as, for example, the upper d band and empty states just above the Fermi surface, in addition to those at conventional critical points. Finally, in Sec. 5, we use the present calculations as a basis for comment on the extent to which the optical properties of the noble metals can be explained on the basis of direct vertical transitions in k space only. This point is of current interest in view of recent comments by Berglund and Spicer,[9] who have called attention to the fact that this conservation law is apparently violated in the optical processes associated with photoemission. An examination of their data along the present lines indicates that, while a part of the structure in the energy distribution of the emitted electrons can probably be explained on the basis of direct transitions, there remains structure which is much more difficult to account for by direct transitions alone.

2. OPTICAL PROPERTIES OF Au

In I, the complex frequency-dependent dielectric constant for Ag and Cu was evaluated over an extended energy range by the well-known Kramers-Kronig analysis of reflectance data.[10] The curves for ϵ_1 and ϵ_2 described three distinct effects, namely, (1) free-electron effects at low energies, characterized by large negative values of ϵ_1, (2) interband transitions which produce structure in ϵ_1 and ϵ_2, and (3) plasma effects which are associated with peaks in the energy-loss function, $-\mathrm{Im}\epsilon^{-1}$. The analysis of $\epsilon(\omega)$ was reasonably straightforward, once it became apparent that for each of these metals the intra- and interband effects could be sepa-

* Supported by the U. S. Advanced Research Projects Agency and Office of Aerospace Research.

† Present address: General Electric Research Laboratory, Schenectady, New York.

[1] H. Ehrenreich and H. R. Philipp, Phys. Rev. **128**, 1622 (1962); hereinafter referred to as I.

[2] B. Segall, Phys. Rev. **125**, 109 (1962).

[3] B. Segall, General Electric Research Laboratory, Report No. 61-RL-2785 G, 1961 (unpublished).

[4] G. A. Burdick, Phys. Rev. **129**, 138 (1963).

[5] J. F. Koch, R. A. Stradling, and A. F. Kip, Phys. Rev. **133**, A240 (1964).

[6] A. S. Joseph and A. C. Thorsen, Phys. Rev. **134**, A979 (1964).

[7] D. Shoenberg, Phil. Trans. Roy. Soc. (London) **255**, 85 (1962).

[8] H. V. Bohm and V. J. Easterling, Phys. Rev. **128**, 1021 (1962).

[9] C. N. Berglund and W. E. Spicer, Phys. Rev. **136**, A1030 (1964); Phys. Rev. **136**, A1044 (1964).

[10] F. C. Jahoda, Phys. Rev. **107**, 1261 (1957); H. R. Philipp and E. A. Taft, Phys. Rev. **113**, 1002 (1959).

rated quantitatively without use of a specific theoretical model. In this connection, it is possible to write the expression for $\epsilon(\omega)$ in the form[1]

$$\epsilon(\omega)=\epsilon^f(\omega)+\delta\epsilon^b(\omega)\,, \tag{1}$$

which separates explicitly the intraband contribution characteristic of free electrons,

$$\epsilon^f(\omega)=1-\omega_{Pa}^2/\omega(\omega+i/\tau_c)\,, \tag{2}$$

from the interband contribution, $\delta\epsilon^b(\omega)$. Here $\omega_{Pa}=[4\pi n_c e^2/m_a]^{1/2}$ is the plasma frequency for free electrons of density n_c and optical mass m_a, and τ_c is the relaxation time for intraband processes.

The separation indicated in Eq. (1) was feasible for these materials, since interband transitions set in at sufficiently high energies where, to a good approximation, $\epsilon_2^f\approx 0$. Hence it was possible to isolate rather unambiguously the free and bound contributions to ϵ_2, noting that, for energies below the gap for interband transitions, $\delta\epsilon_2^b=0$. The Kramers-Kronig relation

$$\delta\epsilon_1^b(\omega)=\frac{1}{\pi\omega}\int_0^\infty \frac{d}{d\omega'}[\omega'\delta\epsilon_2^b(\omega')]\ln\left|\frac{\omega+\omega'}{\omega-\omega'}\right|d\omega' \tag{3}$$

was then used to obtain $\delta\epsilon_1^b$ and $\epsilon_1^f=\epsilon_1(\text{expt})-\delta\epsilon_1^b$ by subtracting the interband contribution from the experimental value.

For each of these metals, the curve for $\epsilon^f(\omega)$ was found to fit accurately the description of the Drude region given by Eq. (2) for free electrons having an average "optical" mass m_a. The interpretation of $\delta\epsilon^b(\omega')$ followed the guide lines of available band calculations. Structure in $\delta\epsilon^b(\omega')$, associated with interband transitions near symmetry points in the Brillouin zone, was identified tentatively with the help of these calculations. In addition, the ability to display simultaneously $\epsilon(\omega)$ and its components greatly facilitated the explanation of certain features in the energy-loss function, $-\text{Im}\epsilon^{-1}$.

As we shall see, the results for Au resemble closely those for Cu.[1] Accordingly, the presentation below will be relatively brief, since it follows the procedures sketched above and the more complete treatment of I. The identification and discussion of interband transitions in Au, as well as Ag and Cu are given in Secs. 3 and 4 and represent a more detailed analysis of the subject than that previously presented.

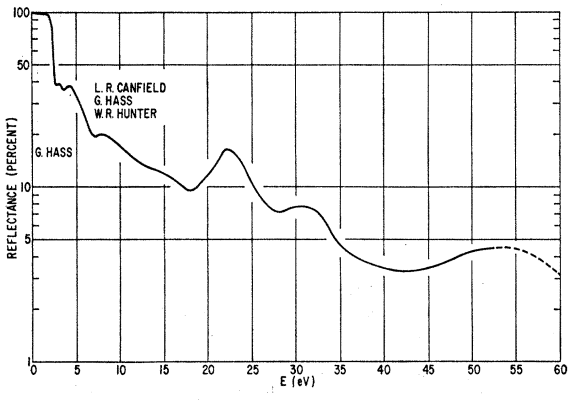

FIG. 1. The spectral dependence of the reflectance of Au. The curve is a composite of the data of Refs. 11 and 12.

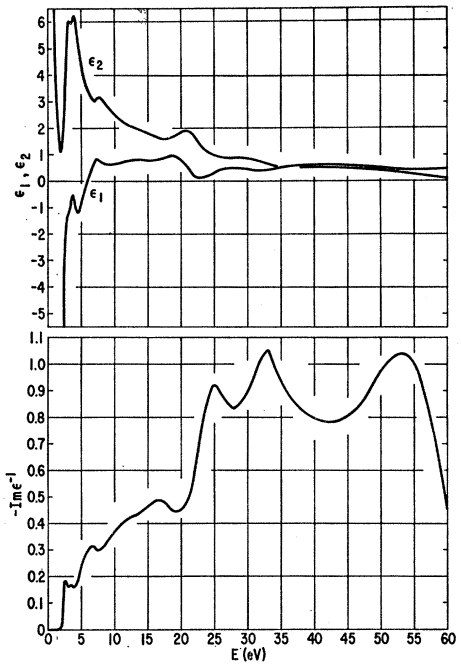

FIG. 2. The spectral dependence of the real and imaginary parts of the dielectric constant ϵ_1 and ϵ_2 and the energy-loss function $-\text{Im}\epsilon^{-1}$ for Au obtained by Kramers-Kronig analyses of the curve of Fig. 1. The extrapolation used is indicated in Ref. 13.

The reflectance spectrum of Au is shown in Fig. 1. These data are a composite of the tabulated values of G. Hass[11] and the recent measurements of Canfield, Hass, and Hunter.[12] Plots of the real and imaginary parts of the dielectric constant ϵ_1 and ϵ_2, as well as the energy loss function $-\text{Im}\epsilon^{-1}$, obtained by Kramers-Kronig analysis of the curve of Fig. 1, are shown in Fig. 2. For this purpose, the reflectance curve was extrapolated[13] at energies above 50 eV to give closely the n and k values reported in Ref. 12 for energies between 6 and 50 eV. The results of Fig. 2 are then also found to agree well with those of Schulz[14] for energies in the range 1 to 3 eV.

The close resemblance between the present results and those for Cu[1] is evident from Fig. 2. The onset of

[11] G. Hass, in *American Institute of Physics Handbook* (McGraw-Hill Book Company, Inc., New York, 1963), Chap. 6, p. 119.

[12] L. R. Canfield, G. Hass, and W. R. Hunter, Colloquium on the Optics of Solid Thin Layers, Marseilles, September 1963 J. Physique **25**, 124 (1964).

[13] The extrapolation is indicated by the dashed line segment in Fig. 1 for energies to 60 eV. In the range 60 to 100 eV, $d\ln R/d\ln\omega=-7.4$. Above 100 eV, the asymptotic slope $d\ln R/d\ln\omega=-4$ was assumed. See H. R. Philipp and H. Ehrenreich, J. Appl. Phys. **35**, 1416 (1964).

[14] L. G. Schulz, Suppl. Phil. Mag. **6**, 102 (1957).

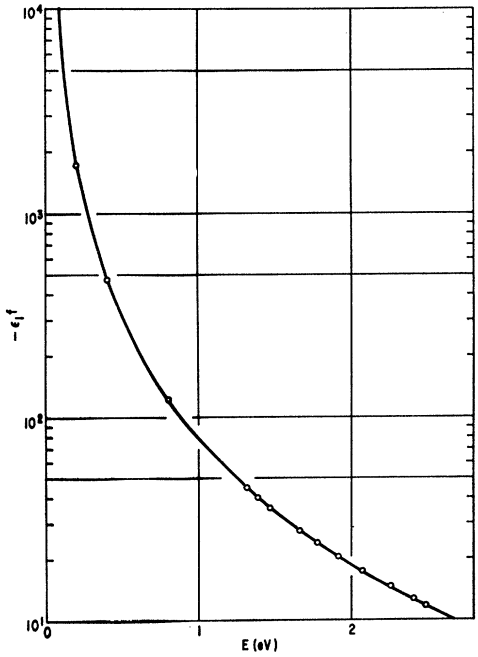

FIG. 3. Comparison of experimental (open circles) and theoretical (solid lines) values of ϵ_1 for Au in the "free electron" region. The experimental points $\epsilon_1^{(f)}=\epsilon_1(\text{expt})-\delta\epsilon_1{}^b$ are adjusted for $\delta\epsilon_1{}^b$ using Eq. (3). The theoretical fit is achieved using Eq. (2) with $\hbar\omega_{Pa}=8.83$ eV. The corresponding value of m_a is 1.04.

interband transitions near 2 eV is associated with the peak in ϵ_1 and the abrupt rise in ϵ_2. It shows up in the reflectance curve as a sharp decrease from the near-unity values which characterize the free-electron region. Near 2 eV, $\epsilon_2{}^f$ is decreasing rapidly according to Eq. (2) and, at higher energies, may be neglected from further consideration. We have thus achieved the desired separation of free and bound contributions to ϵ_2 if we assume that $\delta\epsilon_2{}^b=0$ for all energies below the minimum in the curve for ϵ_2.

The optical mass m_a may now be determined by matching the real part of the intraband component of the dielectric constant as determined from $\epsilon_1{}^f=\epsilon_1(\text{expt})-\delta\epsilon_1{}^b$ and Eq. (3) with values obtained from the Drude formula given by Eq. (2). The result for $n_c=1$ electron per atom and $m_a=1.04$ is shown in Fig. 3. This value of the optical mass is close to the result, $m_a=0.98$, reported by Schulz.[14] Excellent agreement between the two determinations of $\epsilon_1{}^f$ is seen both with respect to magnitude and frequency dependence, even above 2 eV where $\epsilon_1{}^f$ and $\delta\epsilon_1{}^b$ are comparable. This verifies that the separation of the intra- and interband parts of ϵ is reasonable. It should be noted that since $\omega\tau_c\gg1$ for most of the range considered here, the fit in Fig. 3 is practically independent of τ_c.

Now that the intra- and interband contributions to ϵ have been separated, it is convenient to discuss the curve for $-\text{Im}\epsilon^{-1}$, also shown in Fig. 2. Both interband transitions and collective electron effects can give rise to structure in the energy-loss function.[15] It is often possible to discriminate between these by observing the behavior of $\epsilon(\omega)$ in the vicinity of the loss peak, provided broadening effects are not too large. Plasma resonances are distinguished from interband transitions by the fact that, in the former case, both ϵ_1 and ϵ_2 are small near the maximum in the loss function and have positive and negative slope, respectively, whereas, in the latter case, ϵ_1 and ϵ_2 have peaks or structure resembling that of an oscillator. It is not necessary for ϵ_1 to vanish near the plasma frequency. However, when damping is small, that is, $\epsilon_2\ll1$, the condition for plasma resonance is closely $\epsilon_1(\omega_P)=0$. For this case, $-\text{Im}\epsilon^{-1}$ would exhibit a peak of magnitude approximately $1/\epsilon_2(\omega_P)$, a value rather greater than unity. Sharp structure of this kind does not appear in Fig. 2 for Au.[16]

For Au, as well as the other noble metals, one expects to observe a resonance near 9 eV corresponding to the density of free electrons having mass m_a determined earlier. This resonance may be both broadened and shifted in energy due to the presence of interband transitions at higher and lower energies. Weak structure in the curves of $-\text{Im}\epsilon^{-1}$ for Ag and Cu near 7.5 eV was assigned to this resonance. For Au, structure in this region is even weaker. The small peaks near 7 and 15 eV appear to be associated with interband effects.

A second resonance is expected near 30 eV corresponding to collective effects involving the s plus d electrons. The peak near 33 eV may be associated with this resonance, the behavior of ϵ_1 and ϵ_2 being consistent

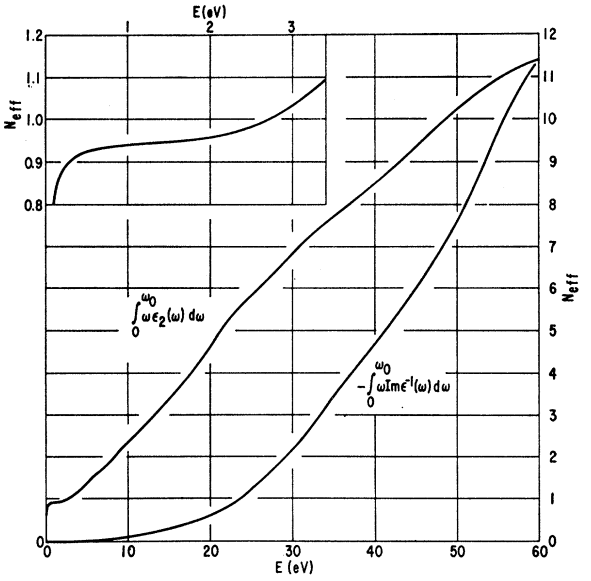

FIG. 4. The effective number of electrons per atom versus E obtained from numerical integration of experimental ϵ_2 and $-\text{Im}\epsilon^{-1}$. The n_{eff} are defined by Eqs. (4) and (5).

[15] Y. H. Ichikawa, Phys. Rev. **109**, 653 (1958).

[16] As pointed out in Ref. 12, the curve of $-\text{Im}\epsilon^{-1}$ is in good agreement with the characteristic energy-loss measurements of J. L. Robins, Proc. Phys. Soc. (London) **78**, 1177 (1961).

with this interpretation. However, this structure in $-\mathrm{Im}\epsilon^{-1}$ is still weak and indeed quite similar to other peaks near 25 and 53 eV, which appear to characterize the curve in the entire energy range to ~60 eV. Hence this assignment must be considered highly speculative.

It is apparent that effects which produce broadening of the optical structure are important in the noble metals. These may well be associated with the presence of the d bands in which one expects electron correlations to be significant. With the single, somewhat remarkable exception of Ag, the separation between collective and interband effects cannot be made unambiguously.

The sum rule

$$\int_0^{\omega_0} \omega\epsilon_2(\omega)d\omega=\left(\frac{2\pi^2Ne^2}{m}\right)n_{\mathrm{eff}}, \tag{4}$$

which yields n_{eff}, the effective number of electrons per atom (in a crystal of atom density N) contributing to the optical properties in the range to ω_0, has been used in previous work on Ag and Cu[1] to indicate energetically the onset of interband transitions, as well as the distribution of oscillator strength for such transitions. A plot of n_{eff} versus $\hbar\omega_0$ is shown in Fig. 4 for Au. It is based on a numerical integration of the experimental values of ϵ_2 in Fig. 2 for energies above about 0.3 eV. At lower energies, where the results of Kramers-Kronig analysis are less reliable, since reflectance data are not available for the longer wavelengths, the integral for n_{eff} was integrated analytically, using Eq. (2) with ω_{Pa} as determined in Fig. 3 and $\tau_c=2.57\times10^{-14}$ sec evaluated from the dc conductivity $\sigma(0)=(1/4\pi)\omega_{Pa}{}^2\tau_c$. For the present purposes, it is sufficient to ignore any possible frequency dependence of τ_c.

In the free-electron region at low energies, n_{eff} rises rapidly and essentially saturates at a value characteristic of $n_c=1$ electron per atom and $m_a=1.04$. The rise above 2 eV is associated with the onset of interband transitions. At still higher energies, n_{eff} increases smoothly, as in the case of Ag and Cu,[1] indicating probably that the oscillator strengths for transitions involving the d electrons are distributed over a wide energy range.

The n_{eff} plot corresponding to the sum rule for the energy loss function, $-\mathrm{Im}\epsilon^{-1}$,

$$-\int_0^{\omega_0} \omega\ \mathrm{Im}\epsilon^{-1}(\omega)d\omega=\left(\frac{2\pi^2Ne^2}{m}\right)n_{\mathrm{eff}} \tag{5}$$

is also shown in Fig. 4. Such a plot has been useful in the case of Al,[17] where the entire energy loss was concentrated in a small energy range near the fundamental plasma resonance or in Ag[1] where there occurs a strong relatively undamped plasma resonance associated with the valence s and d electrons. For Au, this curve is quite smooth, as might be expected from inspection of the energy-loss function plotted in Fig. 2. In the present context, the sum rule on $-\mathrm{Im}\epsilon^{-1}$ is mainly useful in substantiating the internal consistency of the Kramers-Kronig analysis. From inspection of Eqs. (4) and (5), one expects the two integrals to approach the same asymptotic values. This is indeed seen to be the case in Fig. 4 near 60 eV. The two curves coincide at larger energies in the extrapolated region, since $\epsilon_1\to1$ and $\epsilon_2\to0$. Thus, the integrands of Eqs. (4) and (5) are very nearly identical.

[17] H. Ehrenreich, H. R. Philipp, and B. Segall, Phys. Rev. **132**, 1918 (1963).

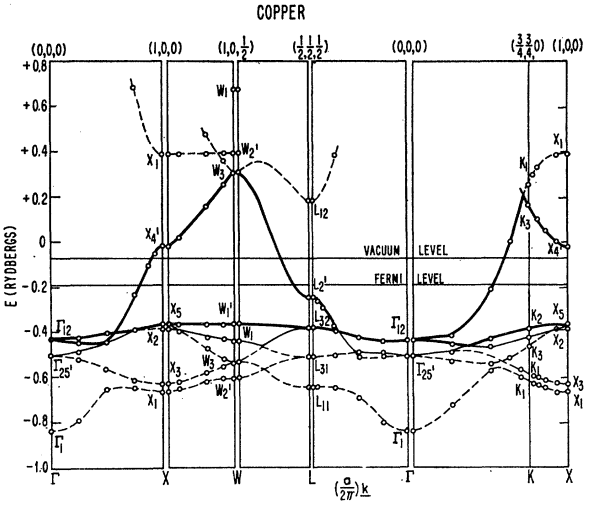

FIG. 5. Calculated band structure of Segall (Ref. 2) for Cu. The heavily drawn bands (bands 5 and 6) give rise to the structure discussed in Secs. 3 and 4. The lightly drawn solid band (band 4) is relevant to the discussion of photoemission in Sec. 5.

3. LOW-ENERGY INTERBAND TRANSITIONS NEAR L

In this section, we will present absolute calculations of $\delta\epsilon_2{}^b$ showing that the lowest frequency interband structure in Cu, Ag, and Au, responsible for the characteristic color of the first and last of these metals, can be associated with the onset of direct transitions between the heavy-mass L_{32} band and the $L_{2'}$ band as the $L_{2'}$ band crosses the Fermi surface. The band structure for Cu is shown[2] in Fig. 5. The bands involved in the transitions in question are the heavy solid curves. The band shapes for Ag are qualitatively similar,[3] but the d bands lie about 2 eV lower, relative to the Fermi energy, than those in Cu. For Au, band energies have been calculated only for a few symmetry points[3]; however, one expects the band structure to be quite similar to that of Cu. This is borne out by the calculations. The various experimental measurements dealing with the Fermi surface[5–8] (see B below), as well as the optical measurements, indicate that the Au band structure and Fermi surface are more like those for Cu than for Ag.

A. Survey of Low-Frequency Interband Structure

The interband contribution to the imaginary part of the dielectric constant for transitions between two

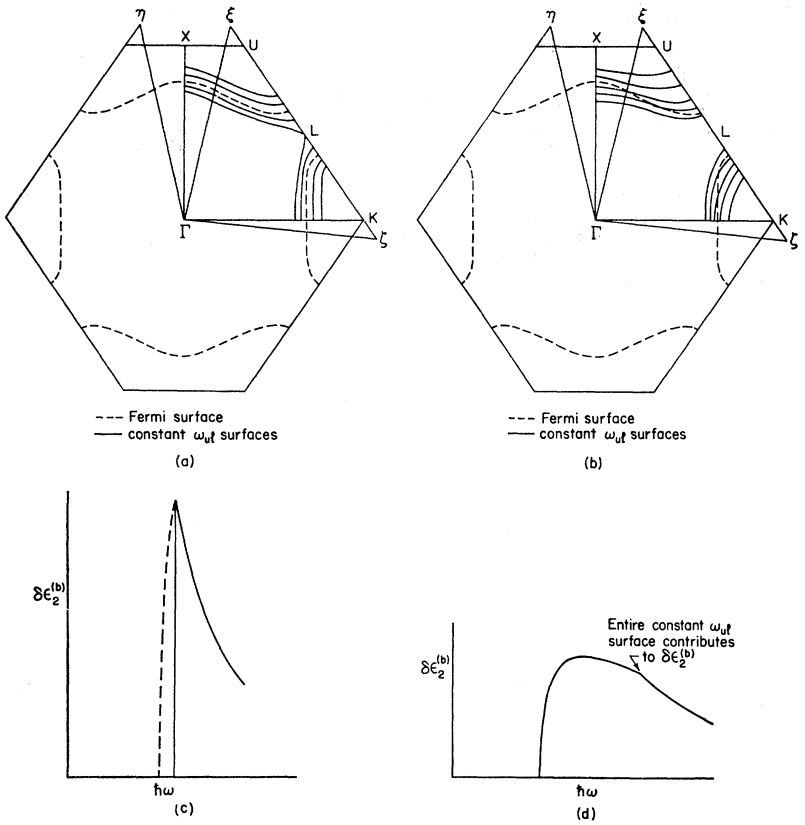

FIG. 6. Uncovering of surfaces of constant ω_{ul} and resultant $\delta\epsilon_2{}^b$: (a) crossing of Fermi surface by surfaces of constant ω_{ul} for flat lower band; (b) crossing of Fermi surface by surfaces of constant ω_{ul} for lower band not flat; (c) solid curve, $\delta\epsilon_2{}^b$ for flat lower band; dashed curve, $\delta\epsilon_2{}^b$ for almost flat lower band; (d) $\delta\epsilon_2{}^b$ for lower band departing significantly from flatness.

bands in a single region of the Brillouin zone is given by

$$\delta\epsilon_2{}^b=\frac{e^2h}{2\pi m}\frac{1}{(\hbar\omega)^2}\int d^3k\frac{2}{m}|P_{ul}{}^\mu|^2\delta(\omega_{ul}-\omega)\,, \qquad (6)$$

$$E_u>E_F,\quad E_l<E_F.$$

Here E_F is the Fermi energy and $P_{ul}{}^\mu=v_a{}^{-1}\int u_{ku}p^\mu u_{kl}d^3x$ is the momentum matrix element, along the direction of propagation of the photon μ, connecting the lower band l with the upper band u at k. Temperature and damping effects have been neglected. Since $\delta\epsilon_1{}^b$ can be obtained using the Kramers-Kronig relation once $\delta\epsilon_2{}^b$ is known, it suffices to consider only $\delta\epsilon_2{}^b$.

For the bands of interest in the limited part of the Brillouin zone to be considered, $|P_{ul}{}^\mu|^2$ may be considered constant to good approximation. Hence,

$$\delta\epsilon_2{}^b=\frac{2\pi^2e^2\hbar E_p}{m}\frac{1}{(\hbar\omega)^2}\rho_{ul}(\omega)\,, \qquad (7)$$

where

$$\rho_{ul}(\omega)=2/(2\pi)^3\int d^3k\delta(\omega_{ul}-\omega)\,, \qquad (8)$$

$$E_u>E_F,\quad E_l<E_F$$

is the joint density of states for vertical transitions between bands l and u and

$$E_p=(2/m)|P_{ul}{}^\mu|^2. \qquad (9)$$

The restrictions involving E_F on the integral insure that the transitions occur only when the lower state is occupied and the upper state is empty.

From (7), we see that, aside from the $1/\omega^2$ factor, the shape of the optical interband structure follows the frequency dependence of $\rho_{ul}(\omega)$. The value of $\rho_{ul}(\omega)$ is proportional to the area of that part of the surface in k space with $\omega_{ul}=\omega$ which satisfies the condition $E_l<E_F$, $E_{\vec{q}}>E_F$. The geometry of the surfaces of constant ω_{ul} follows from the band curvatures as given by the band calculations. The sharpness of structure in $\delta\epsilon_2{}^b$ is determined, in the present context, by the rapidity with which surface in k space, satisfying the conditions $\omega_{ul}=\omega$, $E_l<E_F$, $E_u>E_F$, is exposed as a function of increasing frequency. It is to be emphasized that sharp structure is more commonly produced by Van Hove singularities[18–20] than the present mechanism. However, the case under consideration here is peculiar in that we are dealing with transitions involving a very flat lower band and the Fermi surface at onset. As we shall see, for a nearly flat lower band, the part of the surface of constant ω_{ul} contributing to $\rho_{ul}(\omega)$ increases from zero to the whole surface over a very narrow range of frequency. This leads to an abrupt increase in $\rho_{ul}(\omega)$ and $\delta\epsilon_2{}^{(b)}$.

[18] L. Van Hove, Phys. Rev. **89**, 1189 (1953).
[19] J. C. Phillips, Phys. Chem. Solids **12**, 208 (1960).
[20] D. Brust, Phys. Rev. **134**, A1337 (1964).

For a perfectly flat lower band, surfaces in k space for which ω_{ul} is constant and those for which ω_u is constant coincide. This situation is illustrated schematically in Fig. 6(a), which shows a (110) cross section of the Brillouin zone. The solid curves represent constant ω_{ul} surfaces, for the case of a perfectly flat lower band. The Fermi surface is represented by the dashed curve. It coincides with one of the constant ω_{ul} curves. As a result, $\rho_{ul}(\omega)$ rises abruptly from zero to a finite value when E_u crosses the Fermi surface. The resulting behavior of $\delta\epsilon_2^{(b)}$ is shown by the solid curve in Fig. 6(c). There is a vertical rise in $\delta\epsilon_2^{(b)}$, followed at higher frequency by a decrease. This results both because the area of the contributing ω_{ul} surface decreases as one moves into the corners of the Brillouin zone, and, more importantly, because of the $1/\omega^2$ factor in Eq. (7).

If the lower band is not flat, the constant ω_{ul} surfaces no longer coincide with the constant ω_u surface. This situation is indicated in Fig. 6(b). Again, only the part of a given ω_{ul} surface outside the Fermi surface contributes to $\delta\epsilon_2^{(b)}$. It is obvious that, for this case, the optical transitions are turned on more gradually and the optical structure is correspondingly smeared out. The frequency range for nonzero $\delta\epsilon^{(b)}$ divides itself into two parts: a lower frequency range where the part of the available constant ω_{ul} surface contributing to $\delta\epsilon^{(b)}$ increases with ω_{ul}, and a higher frequency range where the maximum available surface in the Brillouin zone corresponding to each ω_{ul} contributes. If the lower band is almost flat, then the only qualitative change from the ideally flat situation is that the initial rise, while still abrupt, is no longer vertical. This behavior is indicated by the dashed curve in Fig. 6(c). If the lower band departs markedly from flatness, the rise in $\delta\epsilon_2^{(b)}$ will be more gradual. Then one may obtain a situation such as

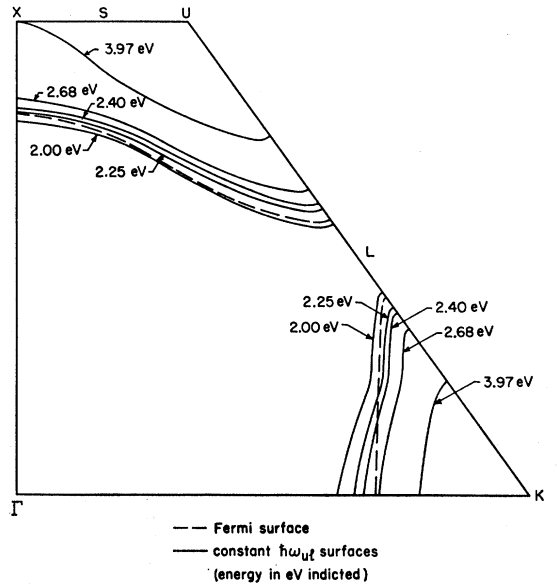

FIG. 7. Cross section in (110) plane of surfaces of constant ω_{ul} and Fermi surface for calculated Cu band structure.

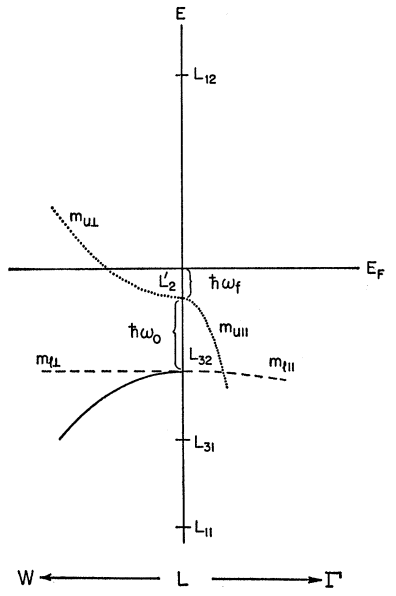

FIG. 8. Band structure near L for the noble metals.

that shown in Fig. 6(d), where the $1/\omega^2$ factor causes the peak in $\delta\epsilon_2^{(b)}$ to occur at frequencies below that for which the maximum available constant ω_{ul} surface contributes. The resulting curve for $\delta\epsilon_2^{(b)}$ will then be much broader and of smaller amplitude.

Turning now to the case of interest here, the constant ω_{ul} surfaces for the $L_{2'}$ and heavy-mass L_{32} bands for Cu obtained from Burdick's bands[4] are shown in Fig. 7. The lower band is indeed almost flat. The Fermi surface therefore nearly coincides with one of the constant ω_{ul} contours over much of the Brillouin zone. Thus one expects sharp optical interband structure with a fairly abrupt onset at about 2.15 eV.

It should be emphasized again that the possibly rapid variation of the joint density of states just discussed is not part of the usual catalog of Van Hove singularities.[18–20] The present effect depends intimately on the existence of a sharp Fermi surface and, for this reason, has no parallel in semiconductors for which the most detailed analyses of optical interband structure have been made. To be sure, Van Hove singularities play an important role in other regions of the spectrum. However, in the present case (cf. Sec. 3.C), transitions associated with the lowest energy optical structure occur in the cone whose cross section is the triangle $\xi\Gamma\zeta$ of Figs. 6(a) and 6(b) for which there are no evident critical points. [Transitions do not occur at L because $E(L_{2'})<E_F$.] On the other hand, the joint density of states connecting X_5 and $X_{4'}$ is representative of a saddle point of the S_2 kind.[18] The vicinity of this point, as represented by cross section $\xi\Gamma\eta$ centered about the $X\Gamma$ axis is not included in the cone $\xi\Gamma\zeta$ and must be treated separately. In I, the upper of the two peaks at low frequencies was assigned to this transition. In Sec. 4, we shall present arguments which support this interpretation.

TABLE I. Band parameters and optical matrix elements.[a]

	Cu	Ag	Au
$\hbar\omega_f = E_F - E(L_{2'})$	0.61 eV	0.30 eV	0.39 eV
neck radius[b]	$0.305\ \pi/a$	$0.214\ \pi/a$	$0.276\ \pi/a$
$m_{u\perp} = m_\perp(L_{2'})$	$0.46\ m_0$	$0.35\ m_0$	$0.44\ m_0$
$m_{u\parallel} = m_\parallel(L_{2'})$	$-0.15\ m_0$	$-0.11\ m_0$	$-0.17\ m_0$
$\hbar\omega_0 = E(L_{2'}) - E(L_{32})$[c]	1.48 eV	3.67 eV	1.96 eV
$m_{l\parallel} = m_\parallel(L_{32})$[d]	$-2.65\ m_0$	$-2.25\ m_0$	$-2.65\ m_0$
E_p	0.58 eV	2.04 eV	0.83 eV

[a] At the completion of the present calculations, the paper of A. S. Joseph and A. C. Thorsen [Phys. Rev. Letters **13**, 9 (1964)] appeared giving different values for $m_\perp(L_{2'})$ and $m_\parallel(L_{2'})$ for Ag and Au than those obtained from Ref. 7. For Ag, Joseph and Thorsen give $m_\perp(L_{2'}) = 0.39 \pm 0.02$ and $m_\perp(L_{2'})/m_\parallel(L_{2'}) = 3.14 \pm 0.10$, in good agreement with Ref. 7. For Au Joseph and Thorsen give $m_\perp(L_{2'}) = 0.29$ and $m_\perp(L_{2'})/m_\parallel(L_{2'}) = 2.38 \pm 0.10$. The smaller value for $m_\perp(L_{2'})$ would give a slightly sharper initial rise for Au, but we expect no qualitative change from that using the value from Ref. 7.

[b] Used in determining $\hbar\omega_f$ for Ag and Au.

[c] $\hbar\omega_0$ determined for Ag and Au from fact that energy for onset of optical structure $= \hbar(\omega_0 + \omega_f)$.

[d] Value for Au assumed equal to that for Cu.

While our present remarks have been directed specifically at Cu, the same arguments concerning the mechanism responsible for the interband structure at onset, as well as the higher peak, will be seen to be applicable also to Ag and Au.

B. Band Parameters

The model for the band structure to be used in considering optical interband structure arising from transitions in the neighborhood of L is shown in Fig. 8. The optical transitions of interest are from the dashed band to the dotted band in the region where the dotted band is above the Fermi energy.

The heavy mass L_{32} band will be assumed to be completely flat in directions transverse to $L\Gamma$. This is consistent with band calculations.

For Cu, the value of E_F and the band separations at L are those calculated by Burdick.[4] Some numerical values are given in Table I. While Segall's results[2] are quite similar to and equally as accurate as Burdick's, differing at most by several tenths of an electron volt, we used Burdick's values because the calculated onset of optical transitions at $\hbar(\omega_0+\omega_f)$ agrees almost perfectly with experiment. In the case of Segall's results, the onset energy would be about 0.50 eV higher.

The values for the transverse and longitudinal[21] masses pertaining to the upper band, $m_{u\perp} = m_\perp(L_{2'})$ and $m_{u\parallel} = m_\parallel(L_{2'})$, are obtained from cyclotron resonance experiments.[5] Here $m_\perp(L_{2'})$ is the cyclotron resonance neck mass when H is parallel to the $L\Gamma$ direction. The longitudinal mass $m_\parallel(L_{2'})$ is obtained by fitting the experimental curve of the variation of the cyclotron mass with angular deviation of the magnetic field direction from the $(1, -1, 1)$ direction in the (110) plane. For an energy surface given by

$$E - E(L_{2'}) = -\hbar^2 k_\parallel^2/2m_\parallel + \hbar^2 k_\perp^2/2m_\perp, \qquad (10)$$

the cyclotron mass m_c is

$$\frac{m_c}{m_0} = \left(\frac{m_0}{m_\perp}\left[\frac{\sin^2\alpha}{(m_\parallel/m_0)} + \frac{\cos^2\alpha}{(m_\perp/m_0)}\right]\right)^{-1/2}, \qquad (11)$$

where α is the angle between H and the $(1, -1, 1)$ direction in the (110) plane, and m_0 is the free-electron mass. The value of $m_\parallel(L_{2'})$ found by fitting the experimental curve of m_c versus α using (11) and also $m_\perp(L_{2'})$ are shown in Table I.[22]

For Ag and Au, present band calculations[3] have not determined the s-d band separations accurately. Accordingly, we use the experimentally determined neck radius and neck mass found from de Haas-van Alphen measurements[7] to find $\hbar\omega_f$. (The neck radii from de Haas-van Alphen measurements are in excellent agreement with the values obtained by magnetoacoustic resonance.[8]) The value of the frequency for the onset of optical structure, obtained from I for Ag and from Sec. 2 for Au, gives $E_F - E(L_{32})$. The values of $\hbar\omega_0$ and $\hbar\omega_f$, as well as the experimental data from which they are derived, are shown in Table I. As we shall show below, absolute calculations using these values of $\hbar\omega_0$ and $\hbar\omega_f$ yield optical structure of the proper shape and magnitude to agree reasonably with experiment. Therefore our use of the optical data to obtain the s-d splitting [i.e., $E(L_{2'}) - E(L_{32})$], when accurate values are not available from band calculations, is self-consistent.

The values of $m_\parallel(L_{2'})$ are obtained by fitting the experimental variation of de Haas-van Alphen period for the neck oscillation $P_n(\alpha)$ with angle of the magnetic field from the $(1, -1, 1)$ direction in the (110) plane.[7] Equation (11) can be used for this purpose by noting that $P_n(\alpha)/P_n(0) = m_c(0)/m_c(\alpha)$.

The remaining masses necessary for the present calculations must be determined from band calculations rather than experiment. For Cu, $m_{l\parallel} = m_\parallel(L_{32})$ is obtained by fitting the curvature of the corresponding band in Burdick's calculations.[4] The same procedure is followed for Ag, using Segall's bands.[3] For Au, band energies are available only for Γ, L, and X. Since, according to various Fermi surface and optical measurements, Au behaves quite similarly to Cu, we assume $m_\parallel(L_{32})$ to be the same as in Cu. These values are shown in Table I.

As an alternative procedure, we could have used the expressions of Fletcher,[23] based on the method of linear combinations of atomic orbitals (LCAO), for the L_{32} band energy $E_k(L_{32})$ as an interpolation formula connecting the more precise band energies calculated at symmetry points. A rough application of this procedure

[21] We use $\parallel$ and $\perp$ throughout to denote band structure quantities which are appropriate, respectively, parallel and perpendicular to the $L\Gamma$ direction.

[22] The value $m_\parallel(L_{2'}) = -0.15\ m_0$ differs from that $(-0.27\ m_0)$ quoted by J. C. Phillips and L. F. Mattheiss [Phys. Rev. Letters **11**, 556 (1963)], presumably obtained by the same procedure using the experimental results of Ref. 5. However, the agreement with the values for $m_\perp(L_{2'})$ and $m_\parallel(L_{2'})$ obtained from de Haas–van Alphen measurements by A. S. Joseph and A. C. Thorsen (Ref. 6) is excellent.

[23] G. C. Fletcher, Proc. Phys. Soc. (London) **65**, 192 (1952).

indicates the results to be quite comparable to those obtained by graphical fitting.

C. Optical Matrix Elements

The only nonvanishing momentum matrix element between L_{32} and $L_{2'}$ involves $p_\perp$. Its value is obtained from the experimentally determined $m_\perp(L_{2'})$, using $\mathbf{k}\cdot\mathbf{p}$ perturbation theory and the assumption that s-d matrix elements at L are equal. We find

$$\frac{m}{m_\perp(L_2')}=1+\frac{2}{m}\sum_{j=L_3}\frac{|(L_j|p_\perp|L_{2'})|^2}{E(L_{2'})-E(L_j)}$$

$$\approx 1+\frac{2E_p}{E(L_{2'})-E(L_{32})}+\frac{2E_p}{E(L_{2'})-E(L_{31})}, \quad (12)$$

where

$$E_p\equiv(2/m)|(L_{2'}|p_\perp|L_{32\text{ heavy mass}})|^2,$$
$$\approx(2/m)|(L_{2'}|p_\perp|L_{32\text{ light mass}})|^2. \quad (13)$$

The last approximate equality in Eq. (13) is exactly satisfied, using the general symmetry properties of $L_{2'}$, for wave functions in the tight binding approximation[23] for both L_{32} and L_{31}. However, using only the general symmetry properties of $L_{2'}$, there is no equivalence between $|(L_{2'}|p_\perp|L_{32})|$ and $|(L_{2'}|p_\perp|L_{31})|$ in the tight-binding approximation.

For Cu, the determination of E_p is straightforward. The band separations are obtained from Ref. 4 and the value of $m_\perp(L_{2'})$ is the experimentally determined one.[5] These values are then substituted into Eq. (12) to obtain E_p. Because the relative positions of the s and d bands depend very sensitively on the crystal potential, it is necessary in the case of Ag and Au to make empirical adjustments of $E(L_{2'})-E(L_{32})$ in order to obtain agreement with the onset of interband transitions. The band separations within the d-band complex, by contrast, are extremely insensitive to the crystal potential. In particular, $E(L_{32})-E(L_{31})$ for Ag and Au, in distinction to $E(L_{2'})-E(L_{32})$, is accurately determined by Segall's band calculations,[3] and can be used in Eq. (12) without further adjustment. For example, in Segall's Hartree-Fock free-ion Ag calculations, $E(L_{32})-E(L_{31})=1.70$ eV, whereas using Hartree functions he obtains 1.71 eV. The calculated values of E_p are given in Table I.

E_p for this transition is seen to be about an order of magnitude smaller than the almost universally constant value ($\sim$1 Ry) characteristic of allowed transitions between band edges which would be degenerate in the absence of a periodic potential.[24] For example, the strong interband transitions in semiconductors are all characterized by E_p of this magnitude.[25] The reason for the difference, in the present case, is that the $L_{32}-L_{2'}$ transition is only quasi-allowed. By this we mean that the $L_{32}-L_{2'}$ transition, while allowed in the solid by general symmetry considerations, is forbidden for L_{32} wave functions in the tight-binding approximation and $L_{2'}$ wave functions expressed as the appropriate symmetrized combination of plane waves. The small nonzero values for E_p result from the fact that the $L_{2'}$ and L_{32} wave functions differ slightly from the symmetrized plane-wave and tight-binding function, respectively.

D. Calculation and Discussion

The contribution to the interband part of the dielectric constant near each of the four equivalent points L is given by Eq. (7). In order to find the total interband contribution, which corresponds, in the case of a cubic crystal, to the equal elements of a diagonal tensor, it is necessary to include an additional factor of 8/3 on the right-hand side of Eq. (7) when E_p is given by Eq. (13). This accounts for the fact that when the contributions of the four (111) directions are added, $|P_{ul^\mu}|^2$ should be replaced by

$$(8/3)|P_{ul}{}^\perp|^2+(4/3)|P_{ul}{}^{||}|^2.$$

In order to evaluate $\rho_{ul}(\omega)$ given by Eq. (8), we define the zero of energy and wave number k at E_F and L, respectively. Thus, in connection with Eq. (8), we may write for the upper band

$$\omega_u=-\omega_f+c_{u\perp}k_\perp{}^2-c_{u||}k_{||}{}^2, \quad (14)$$

where

$$c_{u\perp}=\hbar/2m_{u\perp}, \quad c_{u||}=-\hbar/2m_{u||}. \quad (15)$$

Similarly, for the lower band we have

$$\omega_l=-(\omega_f+\omega_0)-c_{l\perp}k_\perp{}^2-c_{l||}k_{||}{}^2, \quad (16)$$

with

$$c_{l\perp}=-\hbar/2m_{l\perp}, \quad c_{l||}=-\hbar/2m_{l||}. \quad (17)$$

The relevant gap at each k is then given by

$$\omega_{ul}=\omega_0+c_\perp k_\perp{}^2-c_{||}k_{||}{}^2, \quad (18)$$

with

$$c_\perp=c_{u\perp}+c_{l\perp}, \quad c_{||}=c_{u||}-c_{l||}. \quad (19)$$

By means of the transformation

$$k_x=(1/c_\perp{}^{1/2})(\omega_{ul}-\omega_0)^{1/2}\cosh\xi\cos\varphi, \quad (20a)$$

$$k_y=(1/c_\perp{}^{1/2})(\omega_{ul}-\omega_0)^{1/2}\cosh\xi\sin\varphi, \quad (20b)$$

$$k_{||}=(1/c_{||}{}^{1/2})(\omega_{ul}-\omega_0)^{1/2}\sinh\xi, \quad (20c)$$

where $k_\perp{}^2=k_x{}^2+k_y{}^2$, we find

$$\rho_{ul}(\omega)=(\omega-\omega_0)^{1/2}/2\pi^2c_\perp c_{||}{}^{1/2}$$
$$\times(\sinh\xi_{\text{upper}}-\sinh\xi_{\text{lower}}). \quad (21)$$

Here $\sinh\xi_{\text{upper}}$ and $\sinh\xi_{\text{lower}}$ are determined, respectively, from the conditions $E_u>E_F$ and $E_l<E_F$. For the case at hand, $\sinh\xi_{\text{lower}}=0$ and

$$\sinh\xi_{\text{upper}}=\left[\frac{-\omega_f+(c_{u\perp}/c_\perp)(\omega-\omega_0)}{((c_{u||}/c_{||})-(c_{u\perp}/c_\perp))(\omega-\omega_0)}\right]^{1/2}. \quad (22)$$

[24] J. C. Phillips, Phys. Rev. **125**, 1931 (1962).
[25] H. Ehrenreich, J. Appl. Phys. **32**, 2155 (1962).

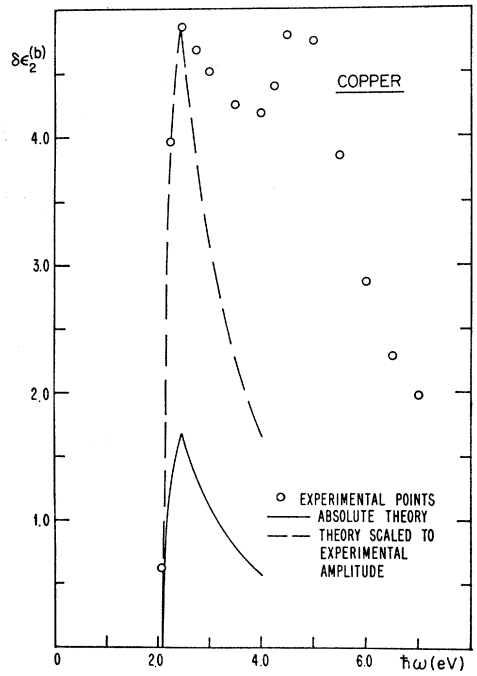

FIG. 9. $\delta\epsilon_2{}^b$ for Cu.

The preceding formulas are valid for any value of m_{Ll}. However, in the present calculation, we assume the heavy mass L_{32} band to be completely flat in directions transverse to $L-\Gamma$. Thus $m_{Ll}=\infty$, and our results simplify, since $c_{ul}/c_l=1$.

There is a restriction, however, that the upper limit given by Eq. (22) can be used only so long as it falls within the maximum volume in k space that can be associated with the neighborhood of a given L point. This maximum volume amounts to one fourth of that for the entire Brillouin zone and is characterized by the cross-section $XULK\Gamma X$ in the (110) plane, shown in Fig. 6, plus the corresponding area on the opposite side of the Brillouin zone.

When this condition is not satisfied, it is necessary to use an alternate cutoff corresponding to the situation discussed in Sec. 3A where the entire surface of constant ω_{ul} lies outside the Fermi surface and contributes to $\delta\epsilon_2{}^{(b)}$. For calculational convenience, we make the approximation that, in this case, the part of the Brillouin zone associated with the transitions at a given L is the cone subtending a solid angle $4\pi/8$ at Γ cross section $\xi\Gamma\zeta$ in Fig. 6 plus the corresponding volume on the opposite side of the Brillouin zone. As can be seen from Fig. 7, this is a reasonable approximation to the behavior of the pertinent constant ω_{ul} surfaces associated with the Cu band structure in the energy range near 2.0 eV. This particular approximation is closely related to Ziman's[26] model for energy surfaces near the Fermi level in the noble metals. The contribution of transitions near X is seen to be excluded. Indeed, Eqs. (14)–(19) for the constant ω_{ul} surfaces are assumed to take adequate account of the region surrounding L, but none at all of the critical point at X. Thus any structure caused by transitions between the heavily drawn bands of Fig. 5 near X will be additive to the structure obtained by the present calculation. These matters are discussed further in Sec. 4.

The condition that the part of k space contributing to the optical transitions falls within the cone defined above is

$$k_x{}^2+k_y{}^2\leq(7/9)(L-k_{11})^2, \tag{23}$$

where L is the ΓL distance ($=\sqrt{3}\pi/a$). Use of the transformation (20) shows that (23) is equivalent to the condition

$$\sinh\xi\leq\sinh\xi_{\text{cone}}, \tag{24}$$

where $\sinh\xi_{\text{cone}}$ is determined by

$$\frac{7c_\perp\sinh^2\xi_{\text{cone}}}{9c_{11}(\sinh^2\xi_{\text{cone}}+1)}\left(\left[\frac{c_{11}\hbar L^2}{\hbar(\omega-\omega_0)}\right]^{1/2}\frac{1}{\sinh\xi_{\text{cone}}}-1\right)^2=1. \tag{25}$$

Then $\rho_{ul}(\omega)$ is determined from (21), with $\sinh\xi_{\text{lower}}=0$, and $\sinh\xi_{\text{upper}}$ given by either (22) or (25), whichever is smaller.

From (7), (21), (22), (25), and the values of parameters given in Sec. 3B, one obtains absolute theoretical curves for the frequency dependence of $\delta\epsilon_2{}^b$ in Cu, Ag, and Au resulting from transitions between the heavy mass L_{32} band and the $L_{2'}$ band in the neighborhood of L.

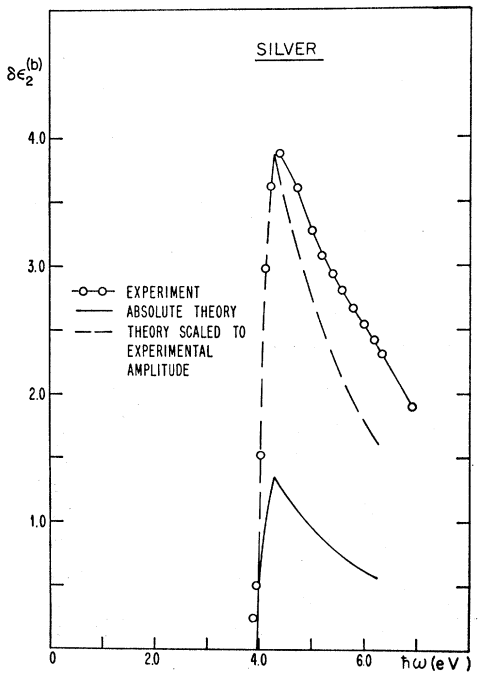

FIG. 10. $\delta\epsilon_2{}^b$ for Ag.

[26] J. M. Ziman, Advan. Phys. 10, 1 (1961).

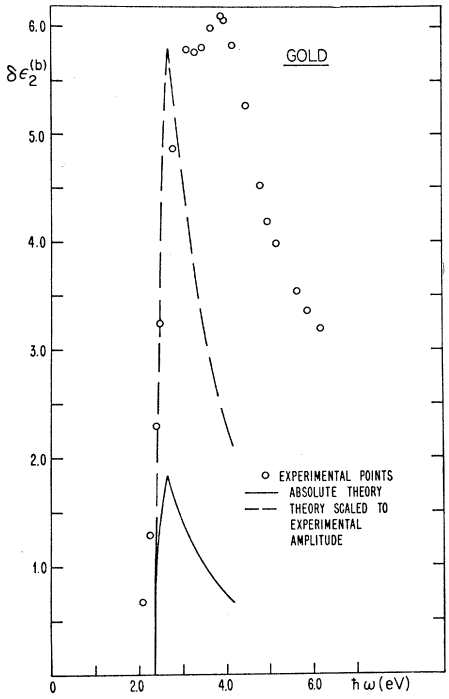

FIG. 11. $\delta\epsilon_2{}^b$ for Au.

These curves are shown in Figs. 9, 10, and 11 together with data for $\delta\epsilon_2{}^b$ deduced directly from experiment. The latter were obtained from $\epsilon_2(\omega)$ as determined by Kramers-Kronig analysis by subtracting $\epsilon_2{}^{(f)}(\omega)$ which is quite small. In the case of Cu and Au, the experimental curves exhibit two well-defined peaks, the lower of which is attributed to the $L_{32}\rightarrow L_{2'}$ transition. The higher peak, which we associate with a transition at X, will be discussed in the following section. The results for Ag reported in I showed only a single peak which rose sharply at low energies and fell off slowly at higher energies. Since the multiple structure observed in Cu and Au would also be expected to occur in Ag, the Kramers-Kronig analysis for this material reported in I was repeated at smaller intervals between successive ω in the region of the peak in order to search for any further structure. The resulting curve, shown in Fig. 10, indeed displays an additional shoulder above 5 eV which was overlooked in I.

In order to permit a better visual comparison of the shape of the experimental and theoretical results, we also show, in each of Figs. 9–11, a curve obtained by multiplying the absolute theoretical results by a scaling factor chosen so as to yield agreement with the amplitude of the experimental peak.

Examination of Figs. 9–11 reveals that the observed structure associated with the lower energy peak is represented quite well by the calculations. The rapid rise of $\delta\epsilon_2{}^b$ at low energies in Cu and Ag is closely reproduced. In the case of Au, the experimental onset is somewhat broader than theoretically expected. Further, the predicted decrease of $\delta\epsilon_2{}^b$ at higher energies is, in all cases, somewhat more rapid than experimentally indicated. Finally, the magnitudes differ by the factors 2.9 for Cu and Ag, and 3.2 for Au, which are almost the same for the three materials.

We begin our discussion of these results by noting that the maximum for each of the three curves occurs at the value of frequency for which $\sinh\xi_{\text{upper}}$ given by (22) equals $\sinh\xi_{\text{cone}}$ given by (25). This corresponds to the frequency at which the entire constant ω_{ul} surface begins to contribute to $\delta\epsilon_2{}^b$. As discussed in Sec. 3A, in general the maximum of $\delta\epsilon_2{}^b$ need not occur at this energy. It occurs so, in the present case, because the lower band is almost flat. If m_l also were infinite, the initial rise in $\delta\epsilon_2{}^b$ would be vertical. This can be seen formally from Eq. (22), where for $c_{ul\parallel}/c_{l\parallel}=c_{ul\perp}/c_{l\perp}=1$, $\sinh\xi_{\text{upper}}$ is infinite for all frequencies of interest ($\omega\geq\omega_0+\omega_f$), and the upper limit on $\sinh\xi$ in Eq. (24) is given by $\sinh\xi_{\text{cone}}$ of Eq. (28) for all frequencies.

Several possible reasons may be advanced for the less abrupt onset of interband transitions in Au. We note first that the two peaks in Au are sufficiently close together, and the second peak sufficiently strong, that the apparent gradual onset may result from a contribution of the higher energy peak. However, it is quite possible that there is a genuine discrepancy between theory and experiment. This may, in part, be due to our assuming a value for $m_{l\parallel}(L_{32})$ in Au equal to that for Cu. If $m_{l\parallel}(L_{32})=-1.09\ m_0$, the theoretical onset of structure would take place over the same frequency range as that observed experimentally. Finally, broadening effects to be discussed below may play a more prominent role in Au than in Cu or Ag. In this regard, it should be noted that the electron-phonon interaction is expected to be greater for Au than for Cu or Ag.[27]

Because of the close proximity and resulting overlap of the two peaks in Ag and Au, quantitative comments concerning the shape and strength of the transition must be confined to Cu. The too rapid falloff characterizing the theoretical peak may be due to several factors. First, no broadening effects have been included in the theory. These would tend to become more important with increasing optical excitation. This circumstance may account for the correspondingly better agreement near the onset of the transition. Second, there will certainly be some contribution in this range from the process giving rise to the peak at 4.5 eV. Third, since the transitions between the bands in question (heavy curves in Fig. 1) are only quasi-allowed for the relevant range of k and energy, the quantity E_p, defined by Eq. (13) may vary appreciably with frequency rather than remaining constant as it does for allowed transitions. In this case, a small variation in the wave functions involved in $P_{ul}(k)$ might have a relatively profound effect on E_p. For example, the theoretical struc-

[27] L. J. Sham and J. M. Ziman, in *Solid State Physics*, edited by F. Seitz and D. Turnbull (Academic Press Inc., New York, 1963), Vol. 15.

ture would be broadened if E_p increased going away from L. As discussed in Sec. 4 below, there is a strong indication that E_p increases going from L toward X. Fourth, there is the possibility that the band model described by Eqs. (14) and (16) leads to an error in the area of the surfaces of constant ω_{ul} contributing to $\delta\epsilon_2{}^b$. It should be recalled, however, that the decrease in $\delta\epsilon_2{}^b$ comes primarily from the $1/\omega^2$ factor and that the effective area of each surface of constant ω_{ul} varies relatively slowly with ω once the whole surface is contributing to $\delta\epsilon_2{}^b$. A crude estimate of the decrease of $\delta\epsilon_2{}^b$ with ω when the surfaces of constant ω_{ul} are obtained from the detailed Cu band structure of Fig. 5 rather than from the approximation of Eqs. (14) and (16) shows that this effect is not likely to be greater than about 15%.

Finally, it should be remembered that the present calculations have all been done within the framework of band theory and the random-phase approximation. One expects effects due to electron correlations to be important, particularly since d bands are involved for the transitions in question here. Such effects would be expected to contribute both to the breadth of the transitions and to their amplitudes. It should be recalled that even for Al,[9] which is considerably simpler and therefore lends itself to more reliable calculations of both the band structure and the optical properties, there were appreciable discrepancies between theory and experiment for both intra- and interband contributions to ϵ. Yet from sum-rule considerations, it was possible to show that the calculations of both contributions was almost perfectly self-consistent. In order to obtain agreement with experiment, it was necessary to shift some of the oscillator strength from the intra- to the interband terms, which is consistent qualitatively, for example, with an increase of effective masses such as might be produced by dressing effects. As already pointed out, in the noble metals one finds that the calculated contribution of the interband terms is also somewhat too small. Application to Cu of the sum rule given by Eq. (4) for $\hbar\omega_0=4$ eV shows that the ratio of the experimental to the absolute theoretical results is approximately 3.5. This magnitude is quite similar to that found for the total interband contribution in Al.[17]

4. TRANSITIONS NEAR X

In I, the higher frequency of the two experimental peaks for Cu (Fig. 9) was tentatively identified with transitions near X associated with the $X_5 \rightarrow X_{4'}$ critical point.[28] As has been discussed in Sec. 3, the calculations of that section omit the volume in the Brillouin zone centered about the ΓX axis with cross-section $\xi\Gamma\eta$ in Fig. 6. Thus the effect of transitions occurring in that part of the Brillouin zone and associated with this critical point will be additive to the structure calculated in Sec. 3.

[28] The $X_2 \rightarrow X_{4'}$ transition is not allowed.

For Cu, the experimental peak in question occurs at 4.50 eV. On the other hand, the $X_5 \rightarrow X_{4'}$ separations calculated by Burdick[4] and Segall[2] are 3.97 and 4.58 eV, respectively. Since equally reliable information is unfortunately not available for Ag and Au, we shall assume Segall's results[3] for these bands to be correct except for the s-d splitting, which is the result most sensitive to the choice of potential in such calculations. The d band, passing through L_{32}, $W_{1'}$, and X_5, will be assumed to move rigidly relative to the s band passing through $L_{2'}$, W_3, and $X_{4'}$. The magnitude of this shift is determined by matching the onset of the interband transitions near L discussed in the previous section with experiment. The $X_5 \rightarrow X_{4'}$ separation determined in this way is 5.75 or 5.65 eV for the Ag bands based on Hartree-Fock or Hartree atomic wave functions, respectively, and 4.15 eV for Au. By comparison, the shoulder in Fig. 10 for Ag, which we associate with this transition, occurs near 5.5 eV, whereas the second experimental peak in Au lies at 3.9 eV. Thus the location of the higher frequency experimental peaks of Figs. 9, 10, and 11 corresponds quite well to the energy difference at the $X_5 \rightarrow X_{4'}$ critical point, and it seems quite reasonable to associate this structure with the transition in question.

For Cu, it is possible to estimate the magnitude and detailed shape of the structure associated with these transitions. As already noted, the energy difference between the heavily drawn bands of Fig. 5 at X has a saddle point of the S_2 kind (maximum in two directions, maximum in one) just as that at L. The pertinent masses can be estimated from Burdick's Cu bands[4] by fitting the curvatures near X. This procedure[29] gives $m_{\parallel}(X_{4'})=-0.16$ m, $m_{\perp}(X_{4'})=0.41$ m and $m_{\parallel}(X_5)=-1.89$ m, $m_{\perp}(X_5)=\infty$. The value of E_p, the energy corresponding to the only nonvanishing momentum matrix elements for the $X_5 \rightarrow X_{4'}$ transitions, can then be estimated by the use of $\mathbf{k}\cdot\mathbf{p}$ perturbation theory, since this interaction determines $m_{\perp}(X_{4'})$. The procedure is the same as that described in Sec. 3C for evaluating E_p between the same bands at L. For the transitions at X, $E_p=2.86$ eV. This value is much larger than the value $E_p=0.58$ eV which applies to transitions between the same bands at L. This marked increase in E_p is consistent with the quasi-allowed nature of the transitions between these bands and contrasts with the nearly constant values characterizing allowed transitions.[25]

The calculation of $\delta\epsilon_2{}^b$ for the higher energy transitions, which include the effects of the $X_5 \rightarrow X_{4'}$ critical point, proceed in the same manner as those described in Sec. 3D for the L transitions. For $\hbar\omega > E(X_{4'}) - E(X_5)$, the same formulas may be used, while for $\hbar\omega < E(X_{4'}) - E(X_5)$ it is a straightforward matter to modify the calculations to take into account the fact

[29] In Sec. 4, $\parallel$ denotes the ΓX direction and $\perp$ denotes the directions perpendicular to it.

that the constant energy difference surfaces for the two bands are hyperboloids of two sheets rather than hyperboloids of one sheet as for $\hbar\omega > E(X_{4'}) - E(X_5)$. It is, of course, just this change in geometry of the energy difference surfaces that leads to the critical-point effects for $\hbar\omega = E(X_{4'}) - E(X_5)$. We make the approximation that the part of the Brillouin zone associated with the transitions at a given X is the cone subtending a solid angle $4\pi/3$ at Γ whose axis is the ΓX direction. By comparison with the energy-difference curves of Fig. 7, we expect this approximation to be reasonable in the vicinity of the $X_5 \rightarrow X_{4'}$ critical point near 4 eV but not for energies near 2.0 eV where the structure discussed in the previous section occurs.

A synthesis of the numerical results obtained in this and the preceding sections is shown in Fig. 12. The reliable portion of the calculations centering around the peak near 4 eV which arises from the $X_5 \rightarrow X_{4'}$ critical point is shown by solid lines, as are the results near 2 eV obtained in Sec. 3. The heavy dashed line joining the two pieces represents a hand-drawn interpolation which is characteristic of what might be obtained from a more accurate calculation. The critical point near X is seen to provide structure in $\delta\epsilon_2{}^b$ of magnitude comparable to that near L in agreement with experiment. We also indicate by the light dashed line how the structure near 2 eV is represented by the calculations of this section. The present results tend to overemphasize the magnitude of the lower frequency peak because of the use of the much larger value of E_p appropriate to the transitions near X.

Despite the elements of agreement between theory and experiment that have just been noted, it should be emphasized again that there are approximations involved in the present calculations that prevent the results from being quantitatively valid. One of the most serious among these is the assumed frequency independence of E_p in the vicinity of L and X, respectively. E_p has, in fact, been seen to vary by almost a factor of 5 in the range between 2 and 4 eV. The inclusion of the actual frequency dependence of E_p in the region surrounding the peaks would appreciably broaden the structure. A similar effect would result from the inclusion of damping effects arising from the finite lifetimes associated with the quasiparticles. Explicit scattering contributions from the electron-electron interactions may also modify the calculated structure.

Comparable calculations of the structure arising from X are not possible for Ag or Au, since there are no band calculations of sufficient detail or accuracy to be useful in the estimate of the pertinent band curvatures. The question as to why this structure, relative to that arising from L, is much weaker in Ag than in Cu, or Au can, however, be answered qualitatively.

There are two ways in which such differences can come about: first, through changes in the band curvatures, and second through changes in the relative magnitude of E_p at X and L. With regard to the first point, one observes that for both the critical point at X and that at L, $\delta\epsilon_2{}^b \propto m_\perp (m_{11})^{1/2}$, where $m_\perp$ and m_{11} are the interband reduced masses, which, however, are almost the same as the s-band masses. For Cu, the ratio of $E(X_{4'}) - E(X_5)$ to $E(L_{2'}) - E(L_{32})$ is larger than for Ag. These separations are the most important energy splittings determining $m_\perp(X_{4'})$ and $m_\perp(L_{2'})$. From this relative change in energy splittings and the consequent change in $m_\perp(X_{4'})/m_\perp(L_{2'})$, one roughly estimates that the ratio of $\delta\epsilon_2{}^b$ from transitions near X to $\delta\epsilon_2{}^b$ from transitions near L is about 1.5 to 2 times larger for Cu than for Ag. The same ratio for Au falls about midway between those for Cu and Ag.

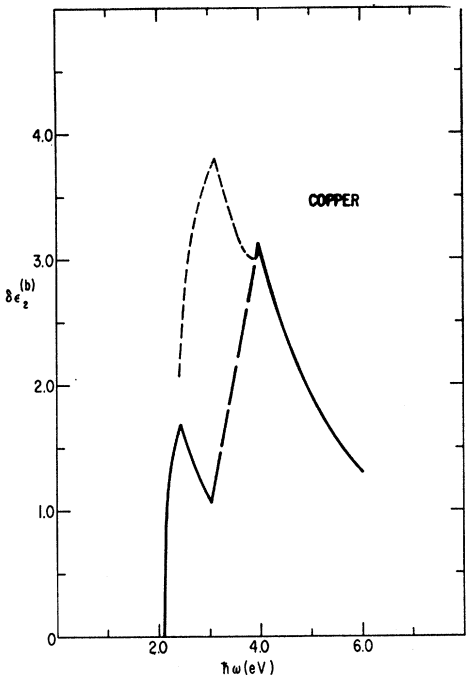

FIG. 12. Calculated $\delta\epsilon_2{}^b$ for Cu. Heavy solid and dashed line shows the synthesis of numerical results for Secs. 3 and 4. Dashed portion refers to interpolation. Light dashed curve shows the inaccurate results for low-energy structure from the calculations of Sec. 4.

The other point to be considered is that the $X_5 \rightarrow X_{4'}$ transition is quasi-allowed. We have already noted the consequent large variation of E_p between L and X for a given metal. Since the ratio of $E(X_{4'}) - E(X_5)$ to $E(L_{2'}) - E(L_{32})$ differs between Cu and Ag, one may expect a corresponding difference between the ratio of E_p at X and L. This would also cause a difference between metals in the relative strength of the two low-frequency peaks in $\delta\epsilon_2{}^b$.

5. DIRECT VERSUS INDIRECT TRANSITIONS

In the preceding sections, we have shown that the low-energy optical interband structure in the noble metals is explicable at least semiquantitatively in terms

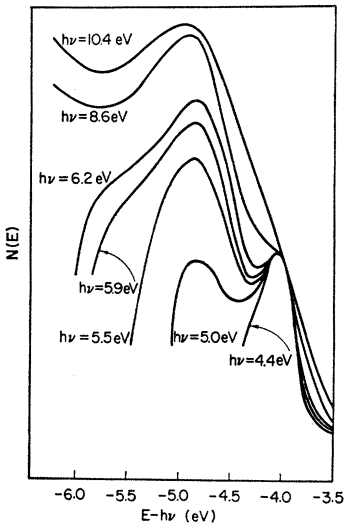

FIG. 13. Energy distribution of photoemitted electrons from Cu plotted versus E (electron energy) $-h\nu$ (photon energy) (This is Fig. 9 of Ref. 9.)

of direct transitions. In this context, it is of interest to examine recent photoemission data for Cu and Ag,[9,30] which were interpreted by Spicer and Berglund on the basis that indirect transitions play a dominant role in the optical absorption processes. Using the insight we have obtained from the preceding calculations, it is possible to examine to what degree the direct processes utilized here explain the observed results. We should stress that while it is valuable to correlate the photoemission results and the ordinary optical absorption, photoemission is basically a more complicated process since in addition to the photon absorption it involves the processes of electron escape from the solid to the vacuum. It is not clear to what extent, if any, this complication obscures identification of initial excitation processes.

The photoemission data of Berglund and Spicer[9,30] for Cu are given in Fig. 13 as a plot of the energy distribution of photoemitted electrons versus electron energy minus photon energy, $E-h\nu$.[31] There are two peaks in the electron-energy distribution which shift linearly with photon energy. The higher energy peak is associated with transitions between the two heavily drawn solid bands in Fig. 5, which we label as bands 5 and 6, respectively.[32] These are just the bands involved in the transitions discussed in Secs. 3 and 4. It is possible to understand the linear shift of this peak with photon energy on the basis of direct optical transitions. Band 5 is seen to be flat through most of the region where band 6 is above the vacuum level. There is a smooth variation of the density of states in the upper band, since there are no critical points in this region except for the point X which lies immediately above the vacuum level and the point W. The effects of the latter are discussed below. Under these circumstances, we expect the photoemission to reflect the sharply peaked density of states of the d band and to shift linearly with $h\nu$, even for direct transitions. Indeed Berglund and Spicer state that for this case of a flat lower band the linear shift does not distinguish between the direct and indirect transition cases.

If the above identification is correct, the band $5 \rightarrow$ band 6 peak should disappear at a photon energy equal to the W_3 to $W_{1'}$ separation. The band calculations of Burdick[4] and Segall[2] indicate this separation to be 8.6 and 9.2 eV, respectively. Figure 13 indeed shows the peak in question to disappear at some photon energy between 8.6 and 10.4 eV, in support of this interpretation. Thus the photoemission behavior in this respect does satisfy a rather strict requirement imposed by the direct transition behavior. It is unlikely that transitions to band 7 would lead to a reappearance of this peak since the optical matrix elements between bands 5 and 7 are probably weaker than those connecting bands 5 and 6. In particular, the transitions $L_{32} \rightarrow L_{12}$ and $X_5 \rightarrow X_1$ are forbidden. For their indirect transition picture, Berglund and Spicer associate the disappearance of this photoemission peak with lifetime broadening. It is quite reasonable to expect such broadening to be present for either indirect or direct transitions, and to increase with increasing excitation energy. The point we stress is that the energy for disappearance is predictable on the basis of direct transitions. However, we cannot rule out a coincidental disappearance due to broadening near this same energy.

There remains the fact, stressed by Berglund and Spicer,[9] that the lower d bands, in particular band 4, are not sufficiently flat to account for the linear shift of the lower electron-energy peak with $h\nu$ on the basis of direct transitions. This indicates that indirect transitions make an appreciable contribution to this peak. However, it does not necessarily imply that indirect transitions predominate. The direct transitions contributing to the lower electron-energy peak would connect bands 3 and 4 as initial states and band 6 as a final state. Since bands 3 and 4 are decidely narrower than the conduction bands, we would expect a peaking in the photoemitted electron energy distribution corresponding to such transitions. It should be emphasized, however, that these bands are considerably broader than band 5. Accordingly, we would expect this peak to be correspondingly broader than the higher energy peak and also not to shift linearly with photon energy to nearly so precise a degree. It is the fact that the peak expected for direct transitions is so broad that may allow indirect transitions, whose width is determined by the relevant part of the d-band complex, to determine the peak location even if the latter do not pre-

[30] W. E. Spicer and C. N. Berglund, Phys. Rev. Letters **12**, 9 (1964).

[31] The curves in Fig. 13 have no common normalization. The proper normalization would be obtained if the area under each curve were proportional to the total yield for that value of $h\nu$ obtained from Fig. 1 of Ref. 30. We are indebted to Professor W. E. Spicer for this information.

[32] Throughout this section we will follow the notation of Ref. 4 and number the bands in order of increasing energy.

dominate over the former. In this case, the peak will again shift uniformly with photon energy.

If the preceding viewpoint is correct and direct transitions predominate, the relative strength of the two photoemission peaks at a given $h\nu$ is expected to be comparable. Indeed, this can be estimated from a consideration of transitions near W between bands 5 and 6, and 4 and 6, respectively. For $h\nu = 7$ and 9 eV, we find that $\delta\epsilon_2{}^b$ for the two kinds of transitions lie within a factor of 2 of each other. It should be noted, however, that such comparable magnitudes could also be obtained if the interaction determining the indirect transition were strongly coupled.

In attempting to account for the apparent failure of k conservation, one might be tempted to invoke the fact that since photoemission effects take place within a short distance of the surface, surface effects are in some way disrupting this selection rule. However, the same could be said of the optical constants as determined by the present reflectance techniques, which are known to be well correlated with bulk properties.

In conclusion, the optical structure for the noble metals in the low-frequency range can be explained quite satisfactorily on the basis of direct interband transitions. While indirect transitions appear to contribute, as suggested by some of the photoemission data, there is no clear experimental evidence indicating that they must be the dominant factor in determining the interband optical properties for the noble metals.

ACKNOWLEDGMENTS

We wish to thank Professor W. E. Spicer for preprints of Ref. 9 and a helpful discussion of both his photoemission work and the present manuscript.

PHYSICAL REVIEW VOLUME 138, NUMBER 2A 19 APRIL 1965

Magnetostriction of Tb Single Crystals*

J. J. RHYNE AND S. LEGVOLD
Institute for Atomic Research and Department of Physics, Iowa State University, Ames, Iowa
(Received 16 November 1964)

The magnetostriction of Tb single crystals has been measured from 4 to 350°K in applied fields up to 30 kOe by strain-gage methods. The temperature dependence of the four magnetostriction constants has been determined under the assumption that the magnetic moment remains in the basal plane. Two of the constants were evaluated by strain measurements as a function of applied-field direction in the basal plane, and the remaining two by isofield magnetostrain measurements and subtraction of the thermal strain extrapolated from the paramagnetic region. The theoretical dependence of the anisotropic basal plane constants on the magnetic moment has been evaluated.

INTRODUCTION

THE magnetostriction of a material is a result of the interaction between the magnetic anisotropy and exchange energies and the elastic energy. In the process of magnetization, if it becomes energetically favorable, the crystal lattice will distort, producing the observed magnetostrain. This strain is normally on the order of 10^{-5} in./in. in ferromagnets such as iron, nickel, and cobalt. In some of the magnetic rare earths however, owing to the large anisotropy energies, the observed magnetostriction is larger by almost 2 orders of magnitude. Most work in the past on the rare earths has been on polycrystalline material because of the lack of single crystals of sufficient size. Single crystals offer considerable advantage in that they permit a direct measurement of crystalline and magnetic anisotropies so that direct correlations with theoretical results can be made. Magnetostriction of the polycrystalline rare earths has been studied by Belov *et al.*,[1] by Nikitin,[2] and by Lee and Alperts.[3] More recent single-crystal studies have been made at this laboratory on Ho,[4] Dy,[4] and Gd.[5] Studies elsewhere have been made by Clark *et al.* on Dy,[6,7] and by Bozorth *et al.* on Gd.[8] The principal strain measurements have been made by the use of strain gages (initially by Goldman and Smoluchowski[9])

* Contribution No. 1609. Work was performed in the Ames Laboratory of the U. S. Atomic Energy Commission.

[1] K. P. Belov, R. Z. Levitin, S. A. Nikitin, and A. V. Ped'ko, Zh. Eksperim. i Teor. Fiz. **40**, 1562 (1961) [English transl.: Soviet Phys.—JETP **13**, 1096 (1961)].
[2] S. A. Nikitin, Zh. Eksperim. i Teor. Fiz. **43**, 31 (1962) [English transl.: Soviet Phys.—JETP **16**, 21 (1963)].
[3] E. W. Lee and L. Alperts, Proc. Phys. Soc. (London) **79**, 977 (1962).
[4] S. Legvold, J. Alstad, and J. Rhyne, Phys. Rev. Letters **10**, 509 (1963).
[5] J. K. Alstad and S. Legvold, J. Appl. Phys. **35**, 1752 (1964).
[6] A. E. Clark, R. M. Bozorth, and B. F. DeSavage, Phys. Letters **5**, 100 (1963).
[7] A. E. Clark, B. F. DeSavage, and E. R. Callen, J. Appl. Phys. **35**, 1028 (1964).
[8] R. M. Bozorth and T. Wakiyama, J. Phys. Soc. Japan **18**, 97 (1963).
[9] J. R. Goldman and R. Smoluchowski, Phys. Rev. **75**, 140 (1949).